3D phenotypic measurement of bitter gourd seedlings based on monocular structured light

Bin Li[1], Weiwei Duan[1], Yanbing Li[1,2], Yande Liu[3], Ge Chen[4], Shangtao Ouyang[1], Youfei Hou[1], Mingjun Zhang[1], Nan Chen[1*]

(1. *Institute of Intelligent Mechanical and Electrical Equipment Innovation, East China Jiaotong University, Nanchang 330013, China*;
2. *School of New Energy Science and Engineering, Xinyu University, Xinyu 338004, Jiangxi, China*;
3. *School of Mechanical and Automotive Engineering, Xiamen University of Technology, Xiamen 361024, Fujian, China*;
4. *Chinese Academy of Agricultural Sciences Institute of Vegetables and Flowers, Beijing 100080, China*)

Abstract: Accurate 3D morphological characterization is critical for precision breeding. However, traditional phenotyping methods suffer from inherent limitations such as low efficiency and loss of dimensional information. To overcome these limitations, this study proposes a robust three-dimensional phenotypic analysis framework based on the monocular Fringe Projection Profilometry (FPP) method. This method is specifically optimized for the high-precision measurement of young plant leaf features. The framework employs a hybrid decoding strategy combining 12-step phase shifting with complementary gray codes to resolve phase ambiguity and reconstruct dense point clouds at sub-millimeter resolution. It addresses the problems of leaf occlusion and adhesion using the section segmentation method. Based on the Oriented Bounding Box (OBB) method of principal component analysis (PCA) and Delaunay triangulation technology, it achieves precise quantification of key phenotypic parameters such as leaf length, width, inclination angle, and area. Systematic verification using 72 bitter gourd seedlings as samples indicates that this method has an extremely high consistency with manual measurement results: the determination coefficients (R^2) for leaf length, leaf width, and leaf inclination angle reach 0.9992, 0.9991, and 0.9933 respectively, with corresponding root mean square errors (RMSE) as low as 0.68 mm, 0.54 mm, and 0.92°, and the R^2 for leaf area reaches 0.9996. This system achieves the complete process from raw scanning to parameter extraction in a low-cost, non-contact, and semi-automated manner, providing reliable data support for the digital perception and intelligent grading standardization of seedling growth dynamics in precision breeding.

Keywords: fringe projection, phase unwrapping, 3D reconstruction, leaf phenotyping
DOI: 10.25165/j.ijabe.20261904.10643

Citation: Li B, Duan W W, Li Y B, Liu Y D, Chen G, Ouyang S T, et al. 3D phenotypic measurement of bitter gourd seedlings based on monocular structured light. Int J Agric & Biol Eng, 2026; 19(4): 191–202.

1 Introduction

High-throughput and non-destructive acquisition of crop phenotypes is the core engine of modern smart agriculture and precision breeding[1]. However, traditional seedling phenotyping primarily relies on destructive sampling and subjective manual measurement. This approach is not only inefficient but also incapable of conducting continuous growth monitoring on individual plants[2]. With technological advancement, image-based phenotyping techniques have gradually supplanted traditional methods[3]. Nevertheless, existing two-dimensional imaging technologies are limited by viewing angles and imaging modes, making it challenging to accurately measure key seedling phenotypic parameters[4,5]. This is particularly true for seedlings, such as bitter gourds, which exhibit high leaf curvature and variable stem inclinations. Accurate analysis of their seedling phenotypes directly determines their subsequent stress resistance and yield. Therefore, developing a technology capable of precisely, non-destructively, and automatically parsing the morphological features of bitter gourd seedlings from a three-dimensional perspective holds significant theoretical value and practical prospects for breaking through breeding bottlenecks and achieving standardized seedling grading.

In recent years, visual-based 3D reconstruction technology is widely hailed as a new approach to addressing this measurement bottleneck. However, in practical applications, the existing solutions are often found to struggle in striking a balance between reconstruction efficiency and spatial details, and there are still many questionable shortcomings identified in terms of measurement accuracy and stability. For example, two high-throughput phenotyping platforms, MVS-Pheno V1 and MVS-Pheno V2, have been developed by Wu et al.[6,7], based on the principles of multi-view stereo 3D reconstruction, enabling automated measurement and phenotype extraction for crops such as maize. However, the reconstruction accuracy was seriously undermined by their huge space requirements and the micro-vibrations caused by turntable rotation, resulting in correlation coefficients of only 0.87 for leaf width and 0.93 for leaf area, which were simply unable to meet the

Received date: 2026-04-15 **Accepted date:** 2026-08-13

Biographies: Bin Li, Professor, research interest: non destructive detection, Email: libingioe@126.com; **Weiwei Duan**, MS, research interest: non-destructive detection in agriculture, Email: dww1677478424@163.com; **Yanbing Li**, PhD, research interest: agricultural detection, Email: liyanbing28@163.com; **Yande Liu**, PhD, research interest: non destructive detection, Email: jxliuyd@163.com; **Ge Chen**, PhD, research interest: agricultural detection, Email: chenge@caas.cn; **Shangtao Ouyang**, PhD candidate, research interest: non destructive detection, Email: ou15779697885@163.com; **Youfei Hou**, PhD candidate, research interest: non destructive detection, Email: houyf11@163.com; **Mingjun Zhang**, MS, research interest: non destructive detection, Email: Aex12138@163.com.
***Corresponding author: Nan Chen**, Professor, research interest: non destructive detection. Institute of Intelligent Mechanical and Electrical Equipment Innovation, East China Jiaotong University, Nanchang 330013, China. Tel: +86-791-87046143, Email: chennan@ecjtu.edu.cn.

measurement requirements for fine phenotypes. A low-cost 3D reconstruction system based on a binocular camera was proposed by Gao et al.[8]. Although its shape extraction determination coefficient was measured to be over 0.91, it was shown to be extremely sensitive to lighting variations. In addition, its high computational complexity and long processing time were regarded as making it completely unsuitable for batch measurement of large-scale seedlings. To improve efficiency, an autonomous point cloud alignment method was presented by Yang et al.[9] and Hong et al.[10] However, although a 0.9676 determination coefficient and 2.08 mm RMSE were obtained by Hong et al. in fruit measurement, the inability to solve single-reconstruction point cloud alignment was identified as their core problem. The leaf point cloud's average absolute distance error was found to be up to 6 mm, and the reconstruction accuracy remained limited. Similarly, Paturkar et al.[11] and Li et al.[12,13] used the motion recovery structure algorithm to extract phenotypic parameters. Although the determination coefficient of leaf length and stem height in Paturkar's study reached 0.97 and 0.99 respectively, and Li's study achieved a determination coefficient of 0.989 in measuring corn leaf length, this method based on multiple views is extremely dependent on multiple image sequences and has extremely high computational complexity. It becomes inadequate when dealing with large-scale sampling scenarios. Recently, the emerging neural rendering technology has also been introduced into this field. Zhu et al.[14] proposed a phenotypic pipeline that combines neural radiance fields with path analysis. However, this method not only has a lengthy post-processing process and is susceptible to environmental interference, but also has poor geometric accuracy. The determination coefficient of the model traits and the real traits fluctuates only between 0.89 and 0.98. In addition, Jiang et al.[15] used three-dimensional Gaussian speckle (3DGS) to enable the measurement of various phenotypic traits, including the number of bolls, volume, plant height, and canopy size. A key limitation of this approach was its reliance on multi-angle acquisition, and it also exhibited low geometric accuracy.

In conclusion, although the existing 3D morphological analysis techniques have made significant progress, they often have to make a trade-off between reconstruction efficiency and spatial details, especially when dealing with the complex non-rigid structures of young plants. To address these technical bottlenecks, this study developed a high-speed 3D measurement system. Firstly, the system employs a hybrid encoding and solving phase strategy to reconstruct the plant point cloud with sub-millimeter accuracy. Then, the cross-sectional segmentation algorithm is used to separate the leaves from the stems and the background. Finally, a framework for extracting phenotypic characteristics is proposed for the leaf phenotypes of bitter gourd. Phenotypic characteristics such as leaf length, leaf width, leaf area, and leaf inclination are directly and precisely quantified from the reconstructed point cloud. This research not only achieves a semi-automated transition from raw scans to precise parameter extraction. Moreover, it also provides a low-cost and high-precision solution for the digital perception of the growth dynamics of seedlings in precision agriculture.

2 Materials and methods

2.1 Overall test plan

A feasible experimental protocol was established to achieve a high-precision and high-density point cloud model. Firstly, a monocular structured-light system was constructed. Next, high-precision system calibration was performed. Subsequently, three-dimensional reconstruction experiments were conducted. Finally, the three-dimensional measurement data were compared with traditional manual measurement results. The schematic diagram of the study is shown in Figure 1: (1) Manual measurement of leaf length and width parameters. (2) Measurement of leaf area using two-dimensional imaging method. (3) Manual measurement of leaf inclination angle.

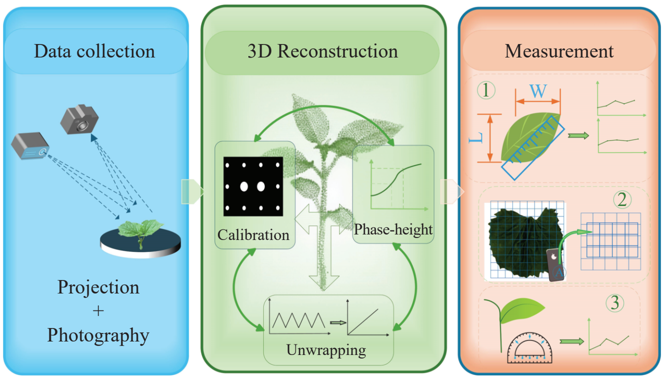

Figure 1 Seedling leaf phenotype measurement schematic diagram

2.2 Experimental materials and platform setup

The 72 bitter gourd seedling samples used in this experiment were provided by the Ganzhou Sub-center of the China Vegetable Quality Standards Center. The height and leaf count of each seedling met the commercial seedling release standards. To ensure the consistency and accuracy of the measured parameters, the analysis was strictly limited to the two largest true leaves on each plant[16]. To systematically evaluate the reliability of 3D reconstruction technology for measuring leaf phenotypic parameters, a procedure was adopted that involved non-destructive 3D reconstruction first, followed by destructive manual measurement.

Existing passive imaging-based 3D reconstruction methods often struggle with objects like seedling leaf, which feature uniform textures and complex geometries[17]. Difficulties in feature matching in these methods often lead to sparse point clouds, lengthy computation times, and compromised accuracy[18]. To address this bottleneck, an active light-coding structured light 3D measurement technique was employed. A novel technical pathway for acquiring high-density, high-precision 3D point clouds of seedlings was enabled by this method, which leverages its capability to actively assign highly distinctive light field codes to objects.

Structured light technology is developed from stereoscopic vision methods, drawing on principles of binocular vision[19]. One camera is replaced by a projector to actively project encoded light spots or fringes onto the target object, thereby artificially creating feature points. The system is primarily composed of a camera, a projector, and a computer. The encoded pattern is projected onto the object's surface, where it was deformed. Images of the distorted pattern are then captured by the camera. Finally, the deformation information is decoded from the pattern by the computer, and, in combination with the system's geometric parameters, the three-dimensional morphology of the object is calculated.

This study establishes a monocular structured light system for seedling phenotyping experiments. The schematic diagram of a monocular structured light system is shown in Figure 2.

The system consisted primarily of: a camera (Baumer HXC20NIR; 2048×1088 resolution), a camera lens (VS-3514H1), a digital projector (TIDLP6500; 1920×1080 resolution), and a computer (equipped with a 12th Gen Intel(R) Core(TM) i5-12400F 2.50 GHz CPU, 32 GB of RAM, and a 64-bit operating system).

The horizontal distance between the camera and projector was set at approximately 240 mm. The camera was positioned about 580 mm from the test sample, while the projector was approximately 540 mm away.

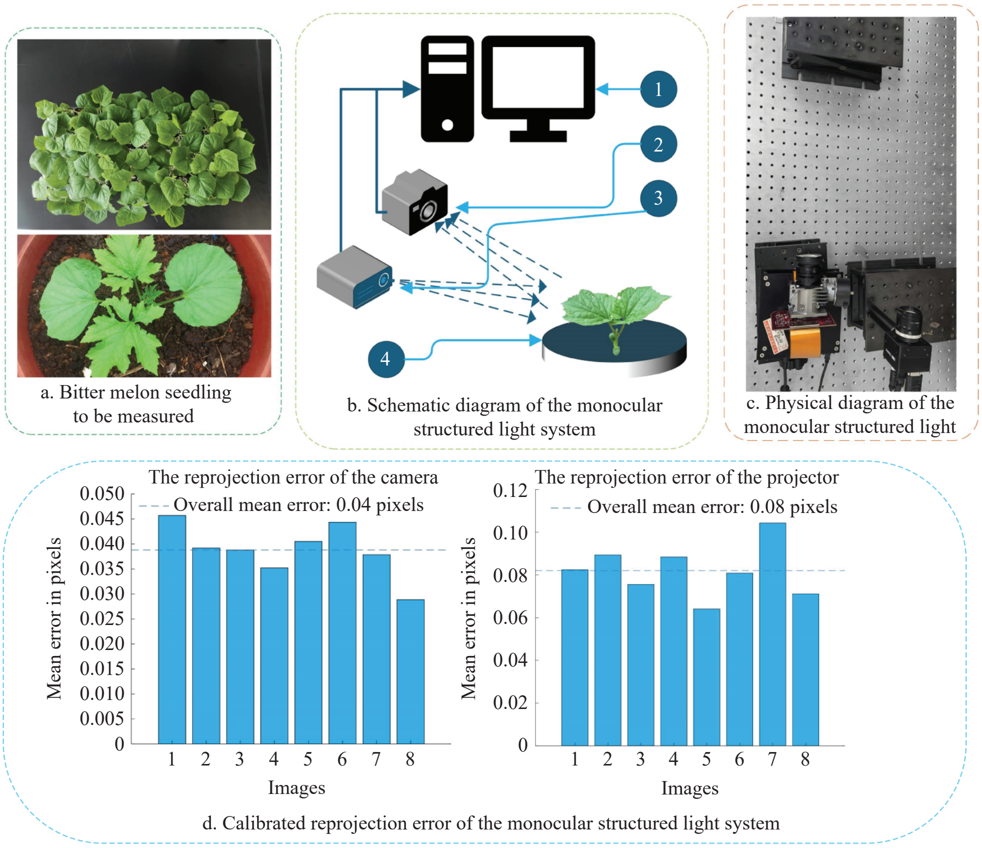

a. Bitter melon seedling to be measured

b. Schematic diagram of the monocular structured light system

c. Physical diagram of the monocular structured light

d. Calibrated reprojection error of the monocular structured light system

Figure 2 Monocular structured light systems

The monocular structured light experiment platform was built according to the schematic diagram. With this arrangement, the pattern from the projector was ensured to be fully projected onto the sample surface and entirely captured by the camera. The experiments were conducted in a dimly lit environment to minimize interference from ambient light on the system.

A calibration procedure was performed to precisely determine the internal parameters (including focal length, principal point, and distortion coefficient) and external parameters (i.e., rotation matrix and translation vector) of the camera and projector. An accurate mapping model from two-dimensional phase information to three-dimensional spatial coordinates was established.

The calibration accuracy was evaluated primarily based on reprojection error. Excellent performance was achieved by the calibration results, with average reprojection errors of 0.04 pixels for the camera and 0.08 pixels for the projector. The reliability of the parameters was thus demonstrated, laying a solid foundation for subsequent high-precision 3D reconstruction.

2.3 High-precision phase acquisition and solution algorithms

2.3.1 Principle of the multi-step phase shift method

In this study, a monocular structured light 3D reconstruction scheme based on FPP was employed. The core principle involved projecting N phase-shifted sinusoidal fringe patterns onto the surface of the object under measurement. The fringe patterns were actively modulated by variations in the surface elevation of the object, resulting in deformations that were directly related to height information. The deformed fringe patterns were subsequently captured by a camera. By combining the acquired fringe patterns with the geometric parameters of the system, the spatial coordinates of the object's surface were determined. The inherent limitations of traditional passive vision methods, which rely on natural texture features for matching, were fundamentally circumvented by this approach. The mathematical expression for the N-step phase shift was:

$$I_k^p(u^p, v^p) = A^p + B^p \cdot \cos[\phi^p(u^p, v^p) + 2\pi k/N] \tag{1}$$

where, N=3, 4, 5, 6, ..., 12 represents the number of phase shift patterns, k=0, 1, 2, ... N–1; A^p represents the background light intensity; B^p represents the modulate amplitude; $\phi^p(u^p, v^p)$ represents the projector initial phase.

These computer-generated phase shift patterns were projected onto the surface of the object under test via a projector, and the deformed phase patterns were captured by the camera. The light intensity of the kth image captured at the camera pixel point (x, y) was:

$$I_k^c(x, y) = A(x, y) + B(x, y) \cdot \cos[\Phi(x, y) + 2\pi k/N] \tag{2}$$

where, $\Phi(x, y)$ represents the absolute phase that carries the height information of the object and the phase objective to be solved. By forming a system of equations from N images, the parcel phase $\varphi(x, y)$ can be solved using the principle of least squares. The formula is as follows:

$$\varphi(x, y) = \arctan\left[\sum_{k=0}^{N-1} I_k^c \sin\left(\frac{2\pi k}{N}\right) \Big/ \sum_{k=0}^{N-1} I_k^c \cos\left(\frac{2\pi k}{N}\right)\right] \tag{3}$$

where, $\varphi(x, y)$ represents the wrapped phase at pixel point (x, y); I_k represents the grayscale value of the phase-shifted sinusoidal stripe pattern at pixel point (x, y) in the kth frame; N represents the number of phase shift steps, which is the number of sine fringes in the projection.

Since the wrapped phase was calculated based on the arctangent function, the calculated values were restricted to the range $(-\pi, \pi]$. Consequently, phase unwrapping was required. A 12-step phase shift was adopted in this study. Compared to the commonly used three-step or four-step phase shifts, phase errors caused by the nonlinear responses of the projector and camera were significantly suppressed by this method, thereby enabling the acquisition of a higher precision wrapped phase $\varphi(x,y)$.

2.3.2 Gray code and complementary gray code combined with phase unwrapping

In order to restore this periodic wrapped phase $\varphi(x,y)$ into an absolute phase corresponding one-to-one with the object surface height, phase unwrapping must be performed. Although traditional temporal phase unwrapping methods are reliable, they require projecting a greater number of fringe sequences with different frequencies, which affects measurement efficiency[20]. Therefore, a high-efficiency and high-robustness gray code-assisted phase unwrapping strategy was adopted. Gray code is defined as a special binary encoding in which only one bit changes between adjacent code words. This characteristic results in the minimization of decoding errors at boundaries. A unique identifier (fringe order k) for each period of the wrapped phase is provided by gray codes, thereby enabling the resolution of periodic ambiguity in phase unwrapping.

In this study, four-bit gray codes plus one complementary gray code were employed for the phase unwrapping process. To uniquely encode 16 fringe periods, four gray code patterns were projected. The binary boundary of the traditional gray code was aligned with the 2π phase jump boundary. In practical applications, weak textures, reflections, noise, and high-gloss areas were exhibited by seedling surfaces. Binarization judgments in these boundary regions are prone to errors, leading to "step jump" errors during phase unwrapping. To address this issue, an additional fifth gray code pattern—the complementary gray code—was projected by this method. The stripe width of this pattern was designed to be half that of the standard phase shift stripe period. Its purpose was defined as generating a set of phase information offset from the original gray code boundaries. As shown in Figure 3a, the multi-step phase-shifted sine grating pattern (1), gray code pattern (2), and complementary gray code pattern (3) are projected onto the surface of the object. A jagged, discontinuous pattern was exhibited by the obtained wrapped phase. A unique periodic sequence number was assigned to each pixel by the addition of gray codes, thereby enabling the unwrapping of the wrapped phase into a continuous absolute phase.

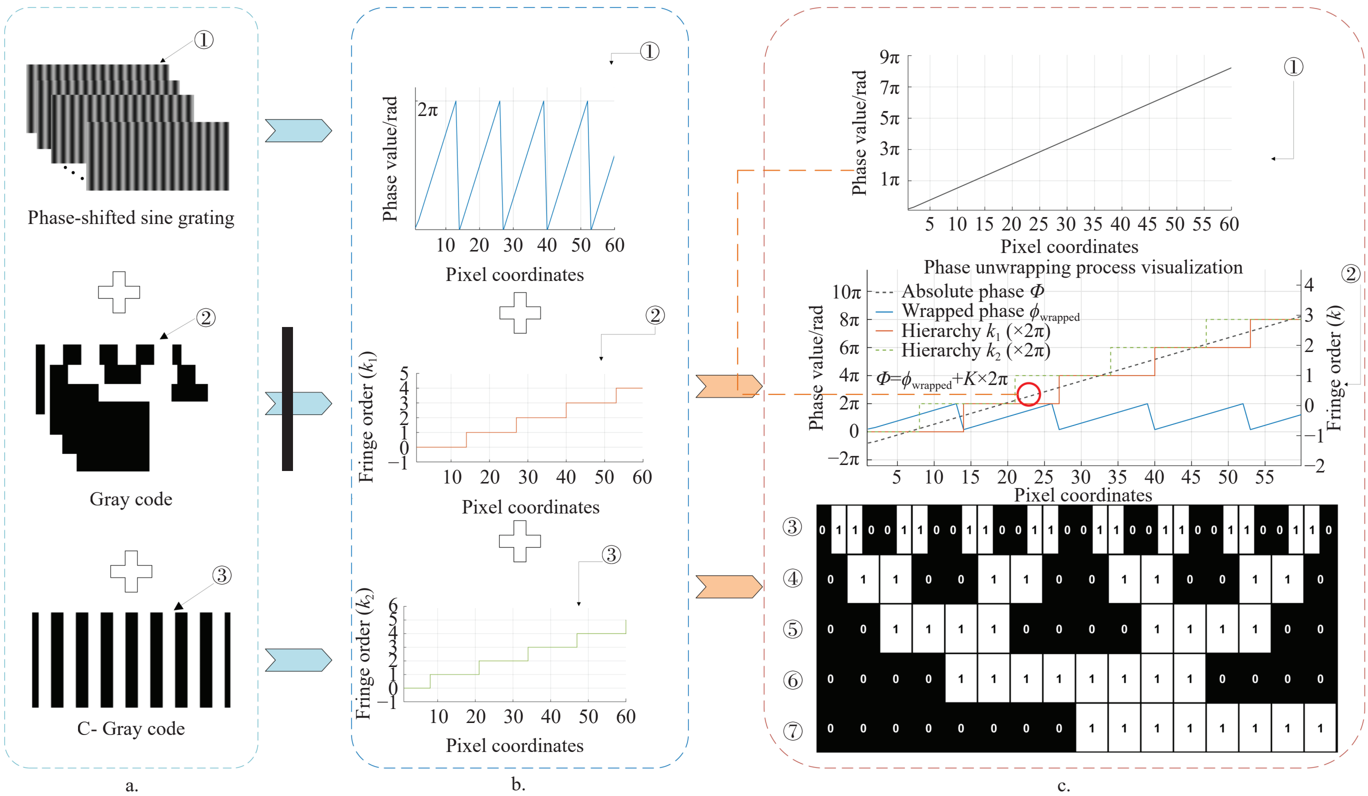

Figure 3 Schematic diagram of the phase settlement process

Additionally, due to ambient light interference and surface reflections, one fully black and one fully white pattern were projected. These were used to filter out ambient light and noise, and to provide binarization thresholds for the gray code images, enabling pixel-wise adaptive thresholding and improving the robustness of gray code decoding.

Two fringe orders were calculated: $k_1(x,y)$ was obtained by decoding the first four gray codes, identifying the primary fringe periods; $k_2(x,y)$ was obtained by decoding the four gray codes and the complementary gray code. Due to the presence of the complementary gray code, the boundary of k_2 was offset by half a period from the boundary of k_1.

Combined with the previously obtained wrapped phase $\varphi(x,y)$ and the two fringe orders k_1, k_2, the absolute phase $\Phi(x,y)$ was calculated using a complementary decoding strategy:

$$\Phi(x,y)=\begin{cases}\varphi(x,y)+2\pi\cdot k_2(x,y), & \text{if } \varphi(x,y)\le -\pi/2\\ \varphi(x,y)+2\pi\cdot k_1(x,y), & \text{if } -\pi/2<\varphi(x,y)<\pi/2\\ \varphi(x,y)+2\pi\cdot k_2(x,y)-2\pi, & \text{if } \varphi(x,y)\ge \pi/2\end{cases} \quad (4)$$

where, $\Phi(x,y)$ represents the decoded absolute phase, $\varphi(x,y)$

represents the obtained wrapped phase, and k_1,k_2 represent the decoding stages of gray code and complementary gray code, respectively.

The core idea of this formula is to avoid error-prone boundaries. When the wrapped phase φ is located in the central stable region $(-\pi/2,\pi/2)$, k_1 is used for calculation. When φ is close to the boundaries $\geq\pi/2$ or $\leq-\pi/2$, k_2 is used. In this way, the phase-unwrapping operation is completely removed from the gray code boundary regions, which had been prone to errors in traditional methods, and order jump errors were eliminated at the source. As shown in Figure 3b, the phase-solving process was diagrammed. The sawtooth-like wrapped phase was converted into a continuous absolute phase by combining order k_1 (from gray code decoding) and order k_2 (from complementary gray code decoding). As shown in Figure 3b, the parcel phase computed by the phase shift pattern, gray code decoding order k_1, and complementary gray code decoding order k_2. In Figure 3c, boundaries offset from the other gray codes were possessed by the complementary gray code shown, providing an auxiliary mechanism to participate in the phase reconstruction process.

To this end, sine grating patterns and gray code patterns were projected in both the vertical and horizontal directions onto the seedling surface. This projection was performed to increase the spatial resolution of the seedling reconstruction. Twelve-step phase shift patterns were projected to ensure phase extraction accuracy, complementary gray codes were projected to resolve phase unwrapping boundary errors, and fully black/white images were projected for adaptive noise filtering and binarization. Combined with dual-direction projection, which further improved spatial resolution, the high precision and robustness of the final 3D reconstruction results were collectively ensured by these measures.

3 Experimental validation and phenotypic measurement

3.1 Reconstructing seedling 3D point clouds

Based on the principle of N-step phase shift and gray code decoding, the 3D point cloud of the seedling was reconstructed using fringe projection profiling. According to Equation (3), the wrapped phase patterns were synthesized from the sinusoidal fringe patterns that had been captured after being deformed by the surface of the measured object, as shown in Figure 4

Figure 4a represents the phase of the parcel obtained from the projected sinusoidal grating pattern. This was a pseudo-color map with significant color jumps at the edges of the object or at sharp changes in height. It was a series of distorted stripe patterns that have been highly modulated by the object surface, and the computed phase values were constrained to be between $(-\pi,\pi]$. Combining the projected gray code pattern and the complementary gray code pattern, the wrapped phase was resolved into a continuous absolute phase. The absolute phase 3D map is shown in Figure 4b.

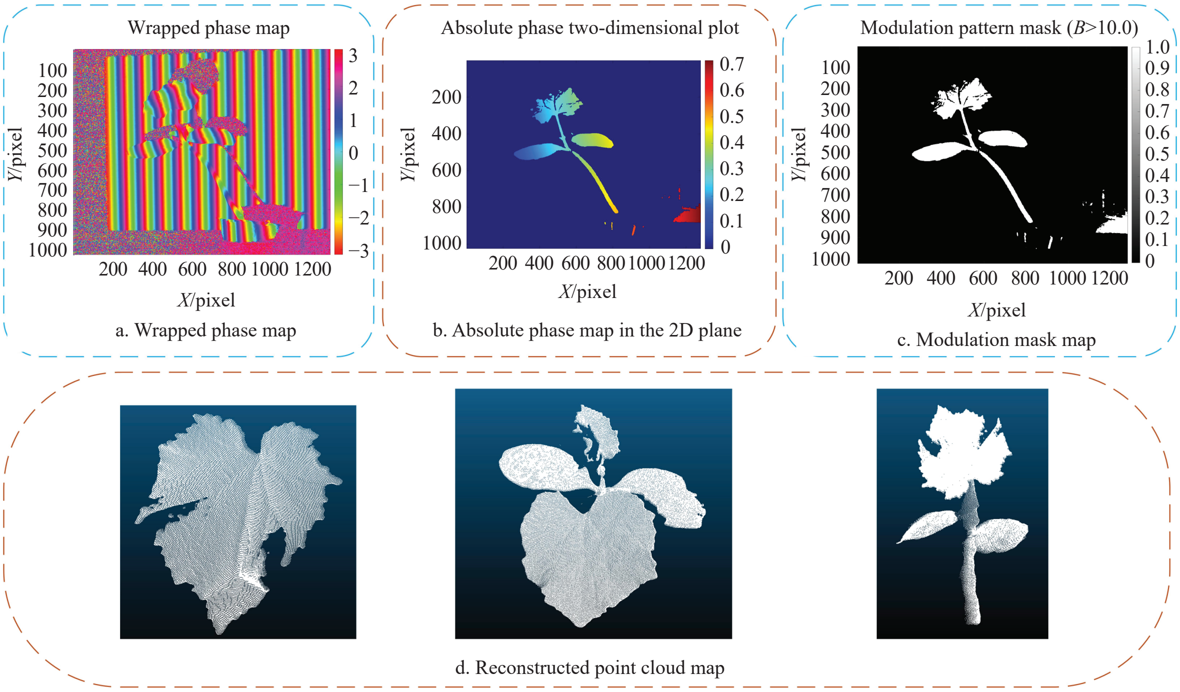

a. Wrapped phase map b. Absolute phase map in the 2D plane c. Modulation mask map

d. Reconstructed point cloud map

Figure 4 Phase unwrapping result

Continuous and smooth color distribution was exhibited by this map. The solved phase was constituted as a continuous, one-to-one phase field corresponding to the height of the object's surface, with each phase having a unique corresponding 3D spatial point. The spatial coordinates of each phase point were directly calculated by combining the parameters of the camera and projector. The modulation pattern mask map is shown in Figure 4c.

The binary image was obtained by threshold filtering based on the modulation regime (Figure 4c). The contrast of the sinusoidal stripe pattern received at each pixel point is reflected by the modulation regime. Better stripe contrast, higher signal-to-noise ratio, and more reliable phase calculation are indicated by a higher modulation regime, and vice versa. The accuracy of the resolution process, characterized by the absence of jump errors and good phase continuity, is reflected by the combination of the absolute phase map and the modulation mask map.

Finally, the 3D morphology of the whole seedling leaves was presented with point cloud data, as shown in Figure 4d.

The point cloud reconstruction was good, the texture was clear, and the reconstruction process was basically successful. The total time required to reconstruct the point cloud of the bitter gourd seedling leaves via the 12-step phase shift method was 15.7 s. As overlapping parts between bitter melon seedling leaves were observed, and the background was also reconstructed, which seriously interfered with the measurement process, therefore it was necessary to separate the leaves of bitter melon seedlings from the seedling point cloud. When common point cloud segmentation algorithms were used to segment the leaf point cloud, the effect was not obvious. Consequently, clustering segmentation was employed to separate the leaf point cloud from the seedling point cloud, thereby facilitating the subsequent characterization of its shape.

4 Three-dimensional geometric definition and computational methods for leaf phenotypic parameters

4.1 Methods for leaf phenotypic parameters

4.1.1 Point cloud preprocessing

After a dense and high-quality 3D point cloud of the whole seedling was obtained, subsequent measurements of leaf phenotypic parameters had to be performed on individual, separated leaf point clouds[21]. Therefore, an interactive cross-sectional segmentation method implemented in Cloud Compare (point cloud processing software) was adopted to accurately extract the target leaf from the complex plant background in this study. The main implementation steps of this scheme were as follows:

Firstly, based on the spatial location and geometric features of the target leaf, a 3D clipping box for the external contour of the leaf is interactively defined. This allows for rapid focusing on the target point cloud and provides an initial operating plane for subsequent precise segmentation. Then, using the clipping tools provided in CloudCompare, one or more cutting planes approximately parallel to the main plane of the leaf are defined. The position and orientation of the planes are adjusted so that they pass through the connection between the leaf and the petiole. The tool automatically retains all point cloud data on one side of the cutting plane while deleting data on the other side. Through these operations, the leaf point cloud is completely segmented from the seedling point cloud.

Individual point cloud data segmented from the whole plant inevitably contains noise introduced during the measurement process[22]. Due to high-reflection areas on the seedling leaf surface, the phase fringe patterns at edges or depth mutations are prone to distortion, and jump errors can be produced by gray code decoding. This leads to calculation errors for individual point phases, resulting in “flying points” deviating from the true surface. Simultaneously, “floating points” may appear in the calculated 3D coordinates at object boundaries due to background light interference. If left unprocessed, these outliers seriously affect the quality of subsequent triangular mesh reconstruction and the accuracy of phenotypic parameter calculations.

To address these issues, the Statistical Outlier Removal (SOR) algorithm was employed to filter the raw point cloud in this study. The core principle of this algorithm was that on a real surface, the local spatial distribution was dense and uniform, whereas outliers exhibit significantly different spatial isolation from surrounding points. The algorithm calculated the average distance from each point to its k nearest neighbors and analyzed the statistical characteristics of the distance distribution for the entire point cloud (such as the mean μ and standard deviation σ). A distance threshold was set (typically $\mu+\alpha\sigma$, where α was a scale factor). Points with an average distance exceeding this threshold were identified as outliers and filtered out. For complete, continuous point cloud surfaces like seedling leaf, the SOR algorithm effectively identified and eliminated abnormal points caused by phase calculation errors or optical interference, significantly improving point cloud data quality and providing robust assurance for subsequent mesh reconstruction and geometric parameter calculation.

4.1.2 Measurement of leaf phenotypic parameters

Leaves are the primary organs for plant photosynthesis. A larger leaf area is correlated with stronger photosynthesis per unit time and more synthesized carbohydrates, providing more adequate nutrients for seedling growth and development[23]. Leaf inclination reflects the spatial extension posture and degree of opening/closing of the leaf. Ideally, the leaf inclination allows the leaf to receive light at the optimal angle and avoid mutual shading[24]. Abnormal leaf inclination may result in sagging or curling of the leaf, directly affecting photosynthetic efficiency. To measure these leaf phenotypic parameters, a generalized method for measuring leaf phenotypes was proposed in this study.

As shown in Figure 5, the measurement of leaf phenotypic parameters included leaf length, leaf width, and leaf inclination. Leaf length is defined as the longest distance from the leaf tip to the leaf root, and leaf width is defined as the longest distance between the two ends of the leaf. Leaf inclination is defined as the angle between the normal vector of the leaf plane and the neutral (vertical) direction.

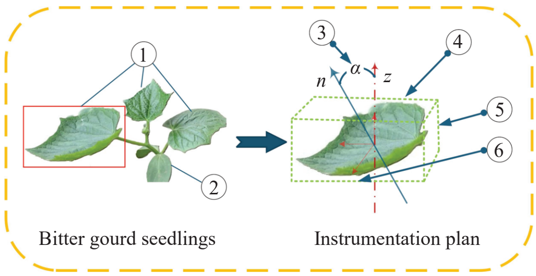

Note: 1. True leaf of bitter gourd seedling; 2. Cotyledon of bitter gourd seedling; 3. Leaf inclination angle; 4. Minimum parcel box; 5. Projected leaf width; 6. Projected leaf length.

Figure 5 Schematic diagram of leaf phenotype measurement

4.1.3 Point cloud measurement scheme based on principal component analysis

In this study, the “three-dimensional Oriented Bounding Box (OBB)” method based on principal component analysis (PCA) was used. This method is employed to determine the main directions of extension of the leaf point cloud in space. The first principal component direction is defined as the leaf length, and the second principal component direction is defined as the leaf width. The OBB is defined as the smallest rectangle along these principal directions that could completely encapsulate the point cloud, and its dimensions were taken as the leaf length and leaf width. For leaf inclination measurements, the normal vector of the leaf point cloud is calculated first. Then the angle between it and the vertical direction is calculated. This angle is used to reflect the extension of the leaf in space. The axes of the wrapping box were defined by utilizing the eigenvalues derived from the covariance matrix of the cluster points. This approach established a local coordinate system aligned with the point distribution, which was essential for the subsequent dimensional measurement.

Since there was no ready-made method to calculate the area of a discrete point cloud, it needed to be converted into a mesh for calculation[25]. Furthermore, because the seedling leaf point cloud was derived from a single-viewpoint scan, the data could be represented as a function $z=f(x,y)$; that was, for every (x,y)

coordinate on the reference plane, there was one and only one corresponding z value. Given this characteristic, a Delaunay 2.5D triangulation algorithm based on principal components was used to fit the mesh plane[26].

The principle of this algorithm assumes a given point cloud set $P=\{p_i\}_{i=1}^{N}$. Firstly, its covariance matrix C was calculated:

$$C = 1/N\sum_{i=1}^{N}(p_i-\bar{p})(p_i-\bar{p})^{\mathrm{T}},\ \ \bar{p} = 1/N\sum_{i=1}^{N}p_i \tag{5}$$

where, N represents the total number of points; p_i represents the coordinate of the $i-th$ 3D point; and $\bar{p}$ represents the centroid of the point cloud and the average value of all point cloud coordinates.

The covariance matrix C, calculated through Equation (5), was used so that the eigenvector corresponding to the smallest eigenvalue was taken as the normal vector n_i of that point. The normal vectors calculated in the three directions were taken as the reference coordinate axes. Subsequently, the center of mass and dimensions of the package box were determined. This approach enabled the measurement of the leaf length and width for the smallest packaging box.

The overall normal vector n of the leaf was obtained by averaging the normal vectors of all points and normalizing them:

$$n_{\text{avg}} = 1/N\sum_{i=1}^{N}n_i \tag{6}$$

Eigen decomposition was performed on the covariance matrix C, and the eigenvector corresponding to the smallest eigenvalue was taken as the normal vector n of the best-fitting plane. This plane was defined as $n\cdot(X-\bar{p})=0$. On this plane, the sum of squared Euclidean distances from all points p_i to the plane was minimized, thereby describing the overall spatial trend of the point cloud.

Then, the 3D point cloud set P was projected orthogonally along the normal vector n onto this fitting plane to obtain a 2D point set $Q=\{q_i\}_{i=1}^{N}$, establishing a mapping relationship between the 3D spatial point cloud and the 2D planar point set.

Subsequently, meshing was performed by executing the Delaunay triangulation algorithm on the 2D point set Q. This algorithm followed the empty circumcircle property, meaning that the circumcircle of any triangle did not contain any other points from the point set Q. This criterion ensured the max-min angle property of the mesh elements, generating triangular facets with excellent morphology.

Finally, the 3D mesh was generated by mapping the vertices of the triangular mesh on the 2D plane back to the original 3D point cloud coordinates, thereby generating the final 3D triangular mesh surface M.

The leaf inclination angle, an important phenotypic parameter, was defined as the angle of the leaf relative to the vertical direction. An accurate calculation method for leaf inclination angle based on the normal vector of three-dimensional point clouds was proposed.

The leaf inclination angle θ was defined as the angle between the normal vector of the leaf surface and the direction of gravity. Its range of values was $[0°, 90°]$. The inclination angle was calculated as follows:

$$\theta = \arccos(|n_x\cdot 0+n_y\cdot 0+n_z\cdot 1|) = \arccos(|n_z|) \tag{7}$$

where, θ is the inclination angle, (°); $n=[n_x,n_y,n_z]^{\mathrm{T}}$ is the unit normal vector on the surface of the leaf. The leaf inclination angle was only related to the z-component of the normal vector.

4.2 Multi-step phase shift experiments and measurements

Through the steps described above, the conversion of physical seedlings into point clouds and mesh maps via fringe projection profiling was fundamentally realized, facilitating subsequent measurement and analysis. According to Equation (4), point cloud data could also be reconstructed by changing the number of phase shift patterns N, provided that $N\geq 3$. Theoretically, as the number of phase shift steps increases, anti-interference capability is strengthened, phase extraction precision is improved, and both reconstruction quality and measurement accuracy are increased. Figure 6 shows a visual comparison of reconstruction results and measurement data of the same leaf under different phase shift steps.

To ensure a fair comparison of the reconstruction performance across different phase shift steps without introducing sample bias, the same set of leaves was reconstructed using the three-step, four-step, six-step, and 12-step phase-shifting methods in this study. The phase shift increments were uniformly distributed across all step numbers (e.g., the 12-step method had a step interval of 30°). Furthermore, to ensure that the image acquisition process did not introduce additional systematic errors, the number of images was varied by maintaining an integer multiple of the step, thereby effectively controlling a single variable. This allowed for a more scientific and clear investigation into the effect of increasing the number of phase shift steps on suppressing systematic nonlinear errors and high-frequency errors.

As shown, Figure 6a presents a point cloud of leaves reconstructed under a three-step phase shift pattern, a grid map, and a real measured point cloud leaf width and leaf length; Figure 6b presents a point cloud of leaves reconstructed under a four-step phase shift pattern, a grid map, and a real measured point cloud leaf width and leaf length; and Figure 6d presents a point cloud reconstructed under a 12-step phase shift pattern, a grid map, and a real measured point cloud leaf width and leaf length.

As shown in the measurement data in Figure 6, the first principal component direction was indicated by the red line, and the length measured along this direction was defined as the leaf length. Conversely, the second principal component direction was indicated by the green line, and the corresponding measured length was defined as the leaf width. For the measurement of leaf inclination, the normal vector of the leaf surface was calculated, and its angle relative to the z-axis was then determined.

The validity and reliability of the proposed 3D measurement method for leaf phenotypic characteristics are verified through an analysis of the experiment. Manual measurements are performed for leaf length, leaf width, and leaf inclination. Tools such as vernier calipers and protractors are used to obtain ground truth values. To mitigate errors that are inevitably introduced during the experimental process, multiple measurements are taken to minimize these errors and ensure that the obtained ground truth values are as accurate as possible. In Table 1 the measured values for leaf width, length, and inclination across 67 sets of data are presented. For leaf area measurement, since manual measurement was cumbersome and prone to error, a mature 2D image method was employed. However, due to the significant curvature of the young bitter gourd leaves, traditional measurement methods were often challenged by numerous difficulties. In this study, the two-dimensional imaging method was employed to obtain the leaf area as the ground-truth reference for comparison. Non-destructive measurement technology was utilized to acquire the original image data of the young bitter gourd leaves. To mitigate the influence of leaf curvature on the measurement results, after the non-destructive measurement, the leaves were cut and flattened. Subsequently, photography of the flattened leaves was performed, and the leaf area was then calculated. The image acquisition was performed using an iPhone 16 Pro Max equipped with a 48-megapixel rear camera. The software utilized for leaf image capture was LeafByte[27-29], an IOS-based application specialized for measuring leaf area.

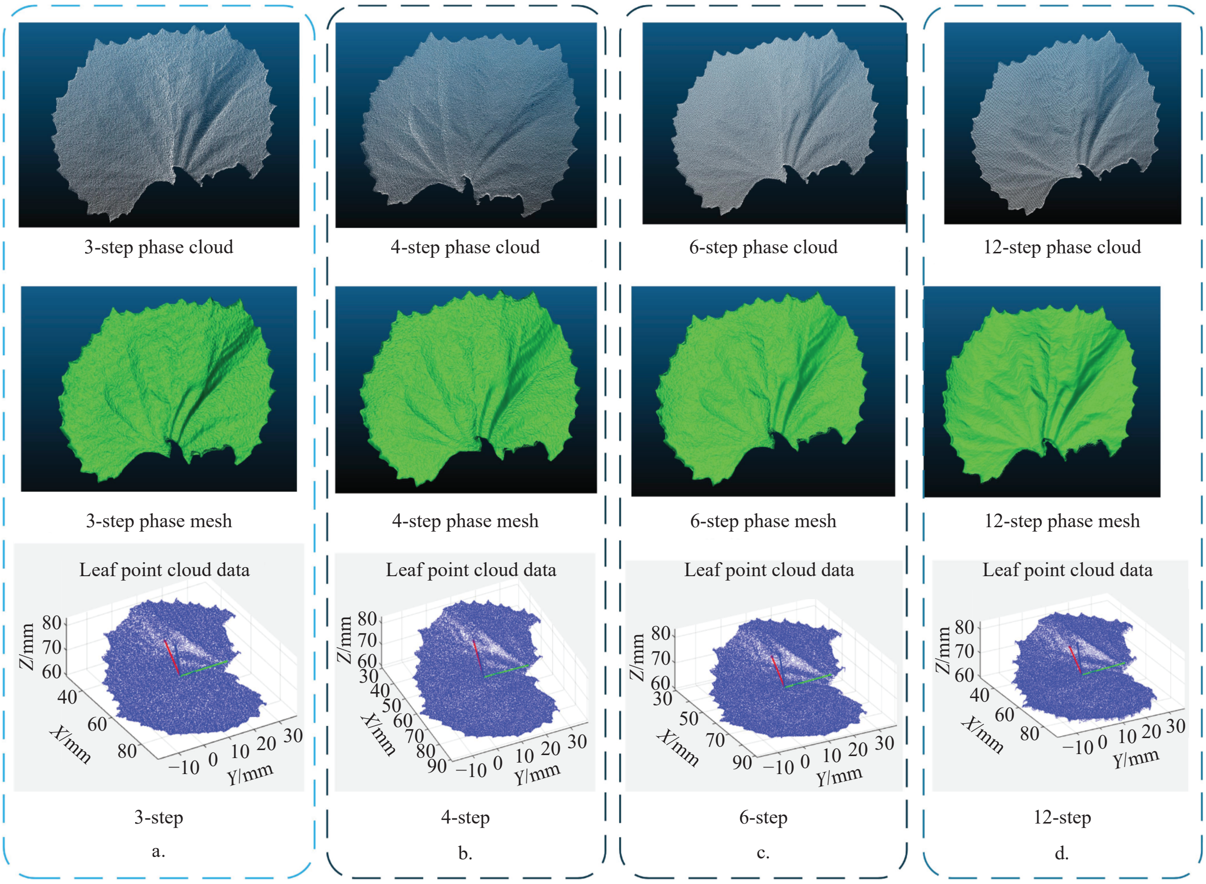

Figure 6 Visual comparison of the point cloud, mesh, and measurement data of the same leaf reconstructed using multiple-step phase-shifting methods (3-step, 4-step, 6-step, and 12-step)

Table 1 Manually measured leaf width, leaf length, and leaf inclination angle values

Seedling number	Leaf width/mm	Leaf length/mm	Leaf inclination/(°)
1	63.4	68.4	13.5
2	54.7	60.1	11.7
3	41.8	49.8	23.6
4	38.3	40.7	17.3
5	61.9	78.0	19.7
6	44.1	56.5	15.3
7	54.2	71.5	11.9
8	56.0	68.7	11.6
9	65.1	72.1	14.3
10	55.3	48.5	12.6

5 Results and discussion

5.1 Analysis of results

The accuracy of reconstructing seedling leaves and measuring their phenotypic parameters using fringe projection profiling was verified by measuring the reconstruction results and comparing them with ground truth values. In this study, the impact of different phase shift steps on the extraction accuracy of seedling leaf phenotypic parameters was primarily evaluated. The coefficient of determination (R^2) and root mean square error (RMSE) were selected as core evaluation metrics to quantitatively analyze four key phenotypic parameters—leaf length, leaf width, leaf inclination, and leaf area—from the two dimensions of linear goodness-of-fit and absolute measurement precision.

Leaf length and leaf width are fundamental morphological parameters describing seedling growth status. Figure 7 shows the regression analysis results of the measured values versus the ground truth values for these two parameters, respectively. Regarding the analysis of leaf length results, an R^2 of 0.9941 and an RMSE of 1.0 mm were obtained using the three-step phase shift algorithm. Although a strong correlation was observed, some data points (particularly in the 50-60 mm range) were found to deviate significantly from the regression line in the scatter plot. These deviations were primarily attributed to the substantial edge noise at the leaf tip and petiole in the point cloud reconstructed with fewer phase shift steps, which led to errors in the Minimum OBB calculation. As the phase shift steps increased to 12, measurement precision improved significantly. The R^2 increased to a near-perfect 0.9992, and the RMSE decreased to 0.68 mm. From the scatter plot, the measurement results were observed to almost perfectly align with the regression line, indicating that the 12-step phase shift accurately restores the axial dimensions of the leaf. Regarding the analysis of leaf width results, high consistency with the leaf length trends was observed in the data. The RMSE for the three-step phase shift was 1.08 mm with an R^2 of 0.9882, while the RMSE for the 12-step phase shift was 0.54 mm with an R^2 of 0.9991. For one-dimensional linear measurements, although the three-step and four-step phase shift methods can meet routine agricultural measurement needs by controlling errors within 1 mm, the 12-step phase shift was considered the optimal choice for fine phenotypic research requiring the capture of minute growth changes.

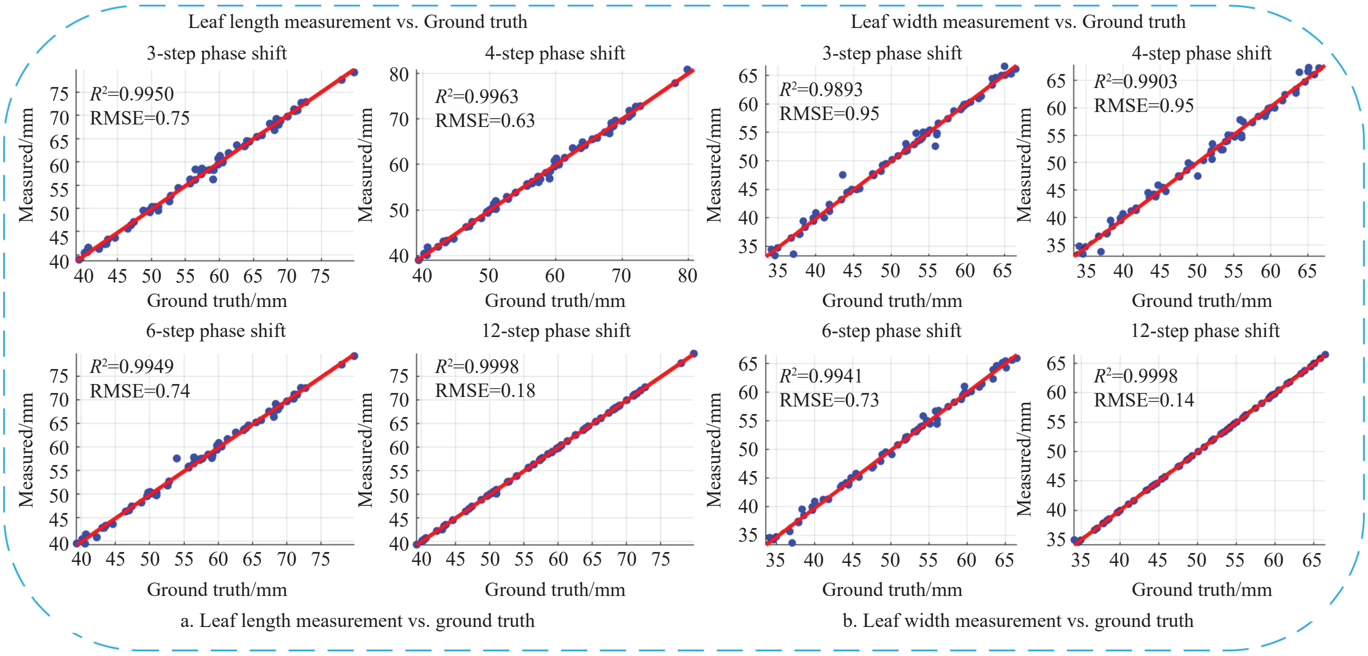

a. Leaf length measurement vs. ground truth b. Leaf width measurement vs. ground truth

Figure 7 Measurement and ground truth data comparison chart of leaf length and leaf width

In plant physiology and agricultural research, accurate leaf area measurement is crucial for assessing plant growth status, photosynthetic efficiency, and resource allocation. Errors can be reduced to some degree by this process, yet certain measurement biases may still be introduced. To more comprehensively evaluate the accuracy of the measurement results, not only were the coefficient of determination R^2 and root mean square error (RMSE) calculated, but Bland-Altman plot analysis was also introduced. Bland-Altman analysis is a commonly used statistical method for assessing the agreement between two measurement techniques. By plotting the differences between the measured and true values against their averages, the accuracy and consistency of the measurement results can be visually demonstrated. The measurement effects achieved by different methods were compared as shown in Figure 8.

As shown in Figure 8a, in the three-step phase shift measurement method, the RMSE was 77.17 mm² and the R^2 was 0.9916. Although the coefficient of determination R^2 was high, the large RMSEs indicated a systematic deviation in area estimation. With the increase in steps to the 12-step phase shift, the RMSE decreased to 29.47 mm², and the R^2 increased to 0.9996. It can be inferred that the leaf point cloud reconstructed using the 12-step phase shift method was smooth, and the fitted mesh model closely approximates the true leaf surface. Bland-Altman analysis of the 12-step phase shift measurement results compared with the true values is illustrated in Figure 8b.

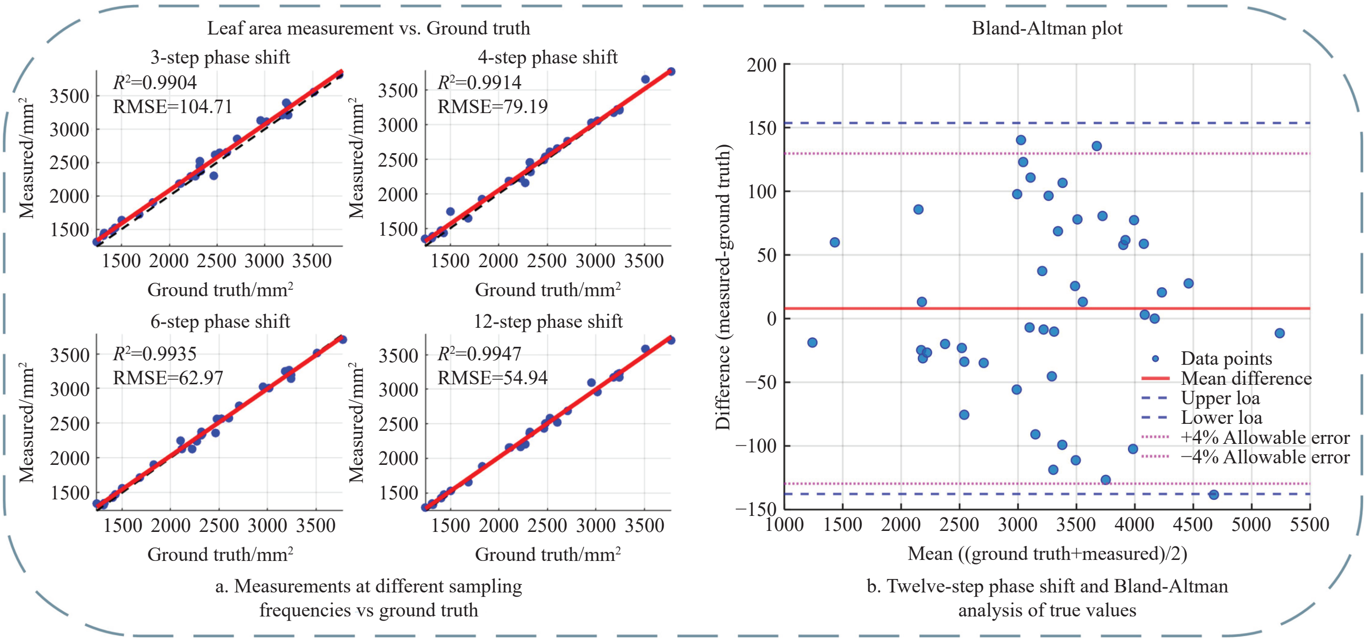

a. Measurements at different sampling frequencies vs ground truth b. Twelve-step phase shift and Bland-Altman analysis of true values

Figure 8 Leaf area measurement vs. ground truth

It can be observed from Figure 8b that all measured points were located within the acceptable error range, which demonstrated that the measurement method employed had high accuracy and reliability.

Leaf inclination is regarded as a parameter reflecting the lightreceiving posture of the plant, and it was found to be the parameter that most clearly differentiated algorithm performance. The relationship between the measurement results obtained by different methods is presented in Figure 9a. In the three-step phase shift mode, the measurement results were observed to exhibit extreme dispersion, the coefficient of determination R^2 was only 0.2988, and the RMSE was as high as 10.57°. A chaotic distribution of the scatter points was observed, indicating that no obvious linear relationship was found between the measured values and the ground truth values. Although an improvement in the measured values was achieved with the four-step and six-step phase shifts, significant deviations were still present, and their scatter distributions remained relatively divergent. The 12-step phase shift yielded the best results, with the RMSE reduced to 0.92° and the R^2 reaching 0.9933. These results confirm that measuring the leaf surface using the 12-step phase shift offers distinct advantages.

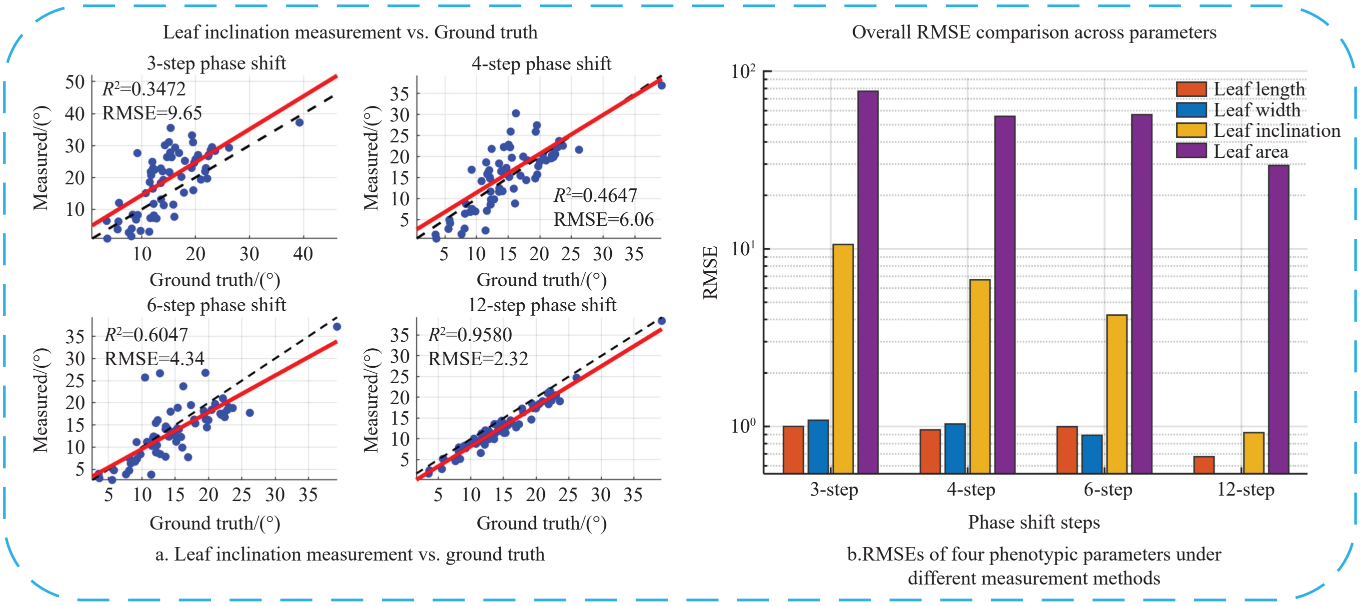

Figure 9 Analysis of the measurement results of leaf inclination and the phenotypic parameter results

5.2 Reliability analysis

Bland-Altman agreement analysis and Bootstrap resampling were introduced to further validate the reliability and robustness of the 12-step phase-shifting method measurement results.

The consistency between the measurements obtained by the 12-step phase-shifting method and the true values measured manually was evaluated using the Bland-Altman method, with an allowable error set at within 4%. The results are listed in Table 2.

Table 2 Evaluation results using the Bland-Altman method

Index	Average difference/mm·(°)$^{-1}$	95% consistency limits/mm·(°)$^{-1}$	Allowable error (4%)	Agreement assessment
Leaf length	–0.59	[–1.23, 0.05]	[–2.32, 2.32]	Good
Leaf width	–0.46	[–1.02, 0.10]	[–2.05, 2.05]	Good
Leaf inclination	–0.72	[–1.87, 0.43]	[–0.54, 0.54]	Moderate

The 95% consistency limits of the leaf length and leaf width were found to be completely within the allowable error range, indicating that good consistency was observed between the two measurement methods. The consistency limit of the leaf inclination angle was found to partially exceed the allowable range; however, high accuracy was still demonstrated by the coefficient of determination (R^2=0.9933) and the root mean square error (RMSE=0.92°). It is suggested that the subsequent measurement algorithm for this parameter be further optimized.

The Bootstrap resampling method was employed to assess the robustness of the 12-step phase shift measurement results, with the resampling frequency set at 1000 times. The mean and standard deviation of the RMSE were calculated through random sampling with replacement, providing a more robust accuracy estimation compared to a single RMSE. The measurement results are listed in Table 3.

Table 3 Assessment results of the Bootstrap resampling method

Index	Sample	Original RMSE/ mm³·(°)$^{-1}$	Bootstrap mean/ mm³·(°)$^{-1}$	Standard deviation/ mm³·(°)$^{-1}$	95% consistency limits/mm³·(°)$^{-1}$
Leaf length	67	0.68	0.67	0.04	[0.59, 0.75]
Leaf width	67	0.54	0.54	0.03	[0.47, 0.61]
Leaf inclination	67	0.92	0.92	0.07	[0.78, 1.06]
Leaf area	28	29.47	29.32	3.35	[22.74, 35.89]

The Bootstrap means of all parameters are highly consistent with the original RMSE, and the standard deviations are extremely small. This indicates that the measurement results have superior stability and repeatability, and are not the accidental manifestations of a single measurement.

6 Discussion

To provide a macroscopic illustration of the performance disparities among various reconstruction strategies, the variations in RMSEs for four phenotypic parameters across different phase shift steps are summarized in Figure 9b. As depicted, the RMSEs of all indicators were consistently diminished as the phase shift steps N were increased. For geometric dimension phenotypes (leaf length, leaf width), the error decrease was relatively gentle, and significant precision advantages were demonstrated by the 12-step phase shift, with the error being controlled at the sub-millimeter level (<0.2 mm). For spatial dimension phenotypes (leaf inclination, leaf area), the results were more sensitive to algorithm robustness. Particularly for the leaf inclination indicator, where the largest error was observed with the three-step phase shift and the smallest with the 12-step, it was concluded that increasing the number of projection steps played a decisive role in suppressing high-frequency phase noise and restoring complex surface features.

Although high-precision measurement results were achieved under controlled lighting conditions in this experiment, ambient light interference and complex plant structures are unavoidable in practical greenhouses or high-throughput platforms. To evaluate the robustness and cross-variety generalization capability of the system under non-ideal conditions, two extended validation experiments were conducted in this study.

First, for the generalization validation across different varieties, the system was applied to the 3D reconstruction of cucumber seedlings. As shown in Figure 10a, although the leaves of cucumber seedlings exhibited severe mutual occlusion and more complex morphology, which increased the difficulty of point cloud segmentation, a high-density 3D point cloud was still successfully reconstructed by the system. This demonstrates that the reconstruction framework based on monocular FPP possesses good applicability across different cucurbit crops.

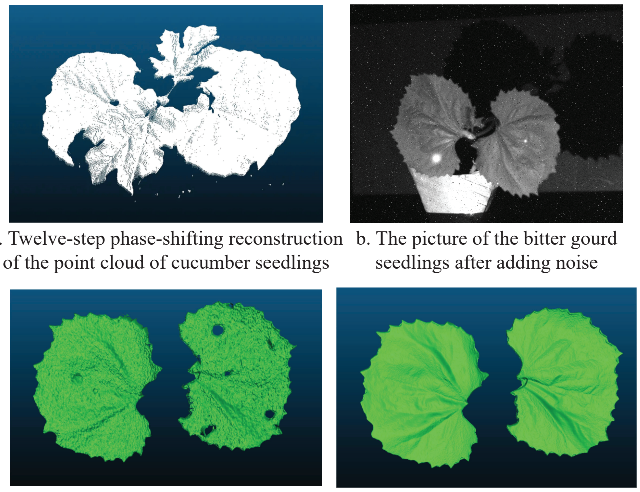

a. Twelve-step phase-shifting reconstruction of the point cloud of cucumber seedlings

b. The picture of the bitter gourd seedlings after adding noise

c. The grid image of bitter gourd seedlings under noise conditions

d. Original picture of bitter gourd seedlings arranged in a grid pattern

Figure 10 System generalization verification and robustness verification

Second, to simulate complex lighting environments, Poisson noise, salt-and-pepper noise, and Gaussian soft light spots (simulating direct ambient light) were introduced into the original phase shift and gray code patterns, as illustrated in Figure 10b. Point cloud reconstruction and parameter extraction were reperformed using the noised images, with the mesh diagrams of bitter gourd seedlings as shown in Figure 10c and 10d.

The results are presented in Table 4. Under noise interference, the error ranges for leaf length and leaf width, which were calculated based on the minimum bounding box method, were 0.41-0.79 mm and 0.42-1.83 mm, respectively. This proves that a high level of robustness can still be maintained even when the system is switched to a strong light environment. However, more significant deviations were observed in leaf inclination and leaf area. This is primarily because the noise induced phase unwrapping errors, which were amplified during the micro-surface normal vector calculation and Delaunay triangulation. This result indicates that when deploying this technology in real greenhouse environments in the future, in addition to adopting hardware optical filters and adaptive projection intensity adjustment, the ambient light resistance capability of the phase shift algorithm needs to be further optimized. Nevertheless, the reliable extraction of geometric scale parameters can still be maintained by this system under complex simulated noise, demonstrating its potential for translation into practical agricultural scenarios.

Table 4 Comparison of measurement values between simulated noise-treated bitter gourd seedlings and original bitter gourd seedlings

Number	Leaf length/mm	Leaf width/mm	Leaf inclination angle/(°)	Leaf area/mm²
1	63.8016	52.1987	11.54	30.9564
1-1	63.5953	54.0312	21.15	47.1454
2	63.6095	53.3517	11.89	29.6108
2-1	64.1893	53.7762	15.63	40.2684

In this study, it was demonstrated that the measurement of leaf inclination was more sensitive to the number of phase shift steps than the measurements of geometric dimensions (length, width). This observation can be attributed to the error propagation mechanism inherent in the phase shift algorithm. In 3D reconstruction, the phase calculation error is closely related to the number of phase shift steps N. Fewer phase shift steps result in weaker suppression capabilities against systematic nonlinear errors and ambient light noise, easily generating periodic "ripple errors." Measurements of leaf length and width primarily rely on the coordinates of extreme points at the point cloud edges; although ripple errors affect surface quality, their impact on edges was relatively limited, thus high R^2 values are still obtained at low step counts. However, for leaf inclination measurement, which is obtained based on calculating the normal vector distribution of the leaf surface, minute ripple-like noise on the surface is amplified by differential operations. This causes drastic deflections in local normal vectors, making the surface appear very rough and resulting in plane fitting distortion. This distortion is clearly observed in the three-step phase shift mode (where R^2 is merely 0.2988). In contrast, the 12-step phase shift, based on the least squares principle, effectively cancels out high-order harmonic interference by increasing the sampling steps N, making the phase calculation smoother. Consequently, the reconstructed leaf surface is smooth and continuous, and the normal vector calculation is accurate, thereby ensuring the high-precision extraction of leaf inclination (R^2 increased to 0.9933) and leaf area.

Although the proposed method demonstrates high accuracy, its limitations must be objectively acknowledged. First, an inherent limitation of structured light technology is its sensitivity to ambient light. Although this experiment is conducted under controlled lighting conditions, strong environmental illumination in real-world greenhouse high-throughput platforms may introduce noise errors during the gray code decoding and phase unwrapping stages. Second, because the current approach relies on multi-frame phase-shifting fringe projection, it is unsuitable for dynamic scenarios, such as plant swaying, and is thus limited to static measurements. Finally, although subsequent parameter extraction has been automated, the front-end point cloud segmentation still requires manual interactive setup of cross-sections, which prevents full end-to-end automation and, to some extent, limits the processing efficiency for extremely large-scale datasets. To address these limitations, future work could explore: (1) integrating single-frame phase shifting with deep learning techniques to handle dynamic scenes; (2) employing optical filters and adaptive projection intensity to mitigate ambient light interference; and (3) leveraging deep learning models (such as PointNet++) to achieve fully automatic leaf segmentation in complex occluded environments.

7 Conclusions

This study developed a semi-automated, non-destructive phenotypic measurement platform for bitter gourd seedlings, enabling automated and high-precision acquisition of key phenotypic parameters. The core contributions are summarized as follows:

This study proposed a high-fidelity 3D reconstruction method based on monocular FPP with a hybrid coding strategy, achieving submillimeter-level 3D reconstruction of seedling leaves.

This study proposed a geometric-aware parameter extraction algorithm based on PCA and OBB, enabling adaptive identification and precise matching of leaf orthogonal axes. The R^2 for leaf length, width, and inclination angle reached 0.9992, 0.9991, and 0.9933, respectively.

This study developed a leaf area calculation scheme based on Delaunay triangulation, and its reliability is verified via Bland-Altman analysis (R^2=0.9996, error band<4%), providing a scientific solution for area measurement of complex-shaped leaves.

Acknowledgements

This work was financially supported by National Key Research and Development Program of China (Grant No. 2024YFD2000603).

[References]

[1] Li L, Zhang Q, Huang D F. A review of imaging techniques for plant phenotyping. Sensors, 2014; 14(11): 20078–20111.
[2] Jin X L, Zarco-Tejada P J, Schmidhalter U, Reynolds M P, Hawkesford M J, Varshney R K. High-throughput estimation of crop traits: a review of ground and aerial phenotyping platforms. IEEE Geosci. Remote Sens. Mag., 2021; 9(1): 200–231.
[3] Jeon Y J, Hong S, Lee T S, Park S H, Song G, Seo M G, et al. Volumetric deep learning-based precision phenotyping of gene-edited tomato for vertical farming. Plant Phenomics, 2025; 7(3): 100095.
[4] Miao Y L, Peng C, Wang L Y, Qiu R C, Li H, Zhang M. Measurement method of maize morphological parameters based on point cloud image conversion. Comput. Electron. Agric., 2022; 199: 107174.
[5] Akhtar M S, Zafar Z, Nawaz R, Fraz M M. Unlocking plant secrets: A systematic review of 3D imaging in plant phenotyping techniques. Comput. Electron. Agric., 2024; 222: 109033.
[6] Wu S, Wen W L, Wang Y J, Fan J C, Wang C Y, Gou W B, et al. MVS-Pheno: a portable and low-cost phenotyping platform for maize shoots using multiview stereo 3D reconstruction. Plant Phenom, 2020; 2020: 1848437.
[7] Wu S, Wen W L, Gou W B, Lu X J, Zhang W Q, Zheng C X, et al. A miniaturized phenotyping platform for individual plants using multi-view stereo 3D reconstruction. Front. Plant Sci., 2022; 13: 897746.
[8] Gao T, Zhu F, Paul P, Sandhu J, Doku H A, Sun J, et al. Novel 3D imaging systems for high-throughput phenotyping of plants. Remote Sens., 2021; 13(11): 2113.
[9] Yang T T, Ye J H, Zhou S Y, Xu A J, Yin J X. 3D reconstruction method for tree seedlings based on point cloud self-registration. Comput. Electron. Agric., 2022; 202: 107210.
[10] Hong S J, Kim J, Lee A. Real-time morphological measurement of oriental melon fruit through multi-depth camera three-dimensional reconstruction. Food Bioprocess Technol, 2024; 17: 5083–5052
[11] Paturkar A, Sen Gupta G, Bailey D. Plant trait measurement in 3D for growth monitoring. Plant Methods, 2022; 18: 59.
[12] Li Y C, Liu J Y, Zhang B, Wang Y G, Yao J F, Zhang X J, et al. Three-dimensional reconstruction and phenotype measurement of maize seedlings based on multi-view image sequences. Front. Plant Sci., 2022; 13: 974339.
[13] Hu C H, Li P P, Pan Z. Phenotyping of poplar seedling leaves based on a 3D visualization method. Int J Agric & Biol Eng, 2018; 11(6): 145–151.
[14] Zhu X H, Huang Z R, Li B. Three-dimensional phenotyping pipeline of potted plants based on neural radiation fields and path segmentation. Plants, 2024; 13(23): 3368.
[15] Jiang L Z, Sun J, Chee P W, Li C Y, Fu L S. Cotton3DGaussians: Multiview 3D Gaussian Splatting for boll mapping and plant architecture analysis. Comput Electron Agric., 2025; 234: 110293.
[16] Sato R, Bizen R, Dong S L, Hayashi S, Wang Z L, Lu J, et al. Vitality evaluation for Pacific oysters (Crassostrea gigas) through heartbeat visualization using image analysis technology. Food Qual. Saf., 2025; 9: fyaf020.
[17] Qin Z, Yu H, Wang C, Guo Y L, Peng Y X, Xu K. Geometric transformer for fast and robust point cloud registration. In: Proceedings of the IEEE/CVF Conference on Computer Vision and Pattern Recognition, New Orleans, LA, USA: IEEE. 2022; pp.11143–11152. doi: 10.1109/CVPR52688.2022.01086.
[18] Li Z P, Wang S S, Su Y P, Yu D Y. A method for measuring strawberry leaf area based on three-dimensional point cloud instance segmentation. IEEE Access, 2025; 13: 25339–25349.
[19] Zhu R S, Sun K, Yan Z Z, Yan X H, Yu J L, Shi J. Analysing the phenotype development of soybean plants using low-cost 3D reconstruction. Sci. Rep., 2020; 10: 7055.
[20] Atefi A, Ge Y, Pitla S, Schnable J. Robotic technologies for high-throughput plant phenotyping: contemporary reviews and future perspectives. Front. Plant Sci., 2021; 12: 611940.
[21] Xie X N, Zhang R R, Guo J, Lu L Y, Pan H Q, Luo X, et al. Strawberry disease detection algorithm based on YOLO11-strawberry. Food Qual. Saf., 2025; 9: fyaf027.
[22] Shen P, Jing X Y, Deng W Z, Jia H Y, Wu T T. PlantGaussian: Exploring 3D Gaussian splatting for cross-time, cross-scene, and realistic 3d plant visualization and beyond. Crop J., 2025; 13(2): 607–618.
[23] Li J, Qi X, Nabaei S H, Liu M, Chen D, Sun Q, Zhang X, et al. A survey on 3D reconstruction techniques in plant phenotyping: from classical methods to neural radiance fields (NeRF), 3D Gaussian splatting (3DGS), and beyond. Plant Phenomics, 2025; 100137. doi: 10.1016/j.plaphe.2025.100137
[24] Zhang C, Kong J J, Wang Z R, Tu C J, Li Y C, Wu D S, et al. Origami-inspired highly stretchable and breathable 3D wearable sensors for in-situ and online monitoring of plant growth and microclimate. Biosens. Bioelectron., 2024; 259: 116379.
[25] Gu J, Zhang Y W, Yin Y X, Wang R X, Deng J W, Zhang B. Surface defect detection of cabbage based on curvature features of 3D point cloud. Front. Plant Sci., 2022; 13: 942040.
[26] Arshad M A, Jubery T, Afful J, Jignasu A, Balu A, Ganapathysubramanian B, et al. Evaluating neural radiance fields for 3d plant geometry reconstruction in field conditions. Plant Phenomics, 2024; 6: 0235. doi: 10.34133/plantphenomics.0235.
[27] Maloof J N, Nozue K, Mumbach M R, Palmer C M. LeafJ: An ImageJ plugin for semi-automated leaf shape measurement. J. Vis. Exp., 2013(71): e50028.
[28] Getman-Pickering Z L, Campbell A, Aflitto N, Grele A, Davis J K, Ugine T A, et al. LeafByte: A mobile application that measures leaf area and herbivory quickly and accurately. Methods Ecol. Evol., 2019; 11(2): 215–221.
[29] Liu Z H, Hu X N, Lu S Y, Xu B, Bai C Y, Ma T, et al. Advances in plant-based raw materials for food 3D printing. Journal of Future Foods, 2025; 5(6): 529–541.